CORRECTED 25 MARCH 2022; SEE FULL TEXT

SCIENCE ADVANCES | RESEARCH ARTICLE

APPLIED SCIENCES AND ENGINEERING

Designing polymeric membranes with coordination chemistry for high-precision ion separations

Ryan M. DuChanois[1,2], Mohammad Heiranian[1], Jason Yang[1], Cassandra J. Porter[1], Qilin Li[2,3,4,5], Xuan Zhang[6], Rafael Verduzco[2,5], Menachem Elimelech[1,2]*

State-of-the-art polymeric membranes are unable to perform the high-precision ion separations needed for technologies essential to a circular economy and clean energy future. Coordinative interactions are a mechanism to increase sorption of a target species into a membrane, but the effects of these interactions on membrane permeability and selectivity are poorly understood. We use a multilayered polymer membrane to assess how ion-membrane binding energies affect membrane permeability of similarly sized cations: Cu^{2+}, Ni^{2+}, Zn^{2+}, Co^{2+}, and Mg^{2+}. We report that metals with higher binding energy to iminodiacetate groups of the polymer more selectively permeate through the membrane in multisalt solutions than single-salt solutions. In contrast, weaker binding species are precluded from diffusing into the polymer membrane, which leads to passage proportional to binding energy and independent of membrane thickness. Our findings demonstrate that selectivity of polymeric membranes can markedly increase by tailoring ion-membrane binding energy and minimizing membrane thickness.

INTRODUCTION

Highly selective separations of specific ionic species are needed to accomplish resource recovery and contaminant removal in water purification processes (*1*, *2*). Unconventional water sources, such as seawater and industrial wastewater, often contain high-value resources or hazardous contaminants that are discarded in complex waste streams (*3*). Reclamation of these species from water could augment mineral supplies in high demand for clean energy technologies (e.g., lithium, uranium, and copper) and isolate toxic species from waste streams before disposal or additional treatment (e.g., nitrate and boron) (*4*, *5*). A continuous process that extracts target ionic species from water would be groundbreaking for the water purification sector by further promoting a circular economy, protecting the environment, and producing safer water.

Biological ion channels provide key insights into the chemical and structural design features needed for a continuous membrane process that separates similar ions. In the K^+ channel, for instance, a narrow, 12-Å-long selectivity filter forces ions to remove their solvation shell, which is associated with an ion-specific energy penalty (*6*). For K^+, this energy penalty is offset by specific and reversible (coordinative) interactions from binding sites along the selectivity filter (*6*, *7*). For Na^+, coordinative interactions with the binding site are less energetically favorable. Smaller ions like Na^+ have larger energy penalties for dehydration, and ligands within the channel are less capable of stabilizing these species (*8*, *9*). Such mechanisms yield a K^+/Na^+ selectivity up to 10^4 (*9*), which is markedly higher than current synthetic membranes.

Polymeric membranes are the most prominent separation technology in desalination, galvanic cells, and electrolytic cells (*10*), but they are unable to effectively separate a single ionic species from a complex aqueous mixture. Polymeric materials are limited by the heterogeneity and dynamic behavior of free volume elements, which precludes ion sieving and establishes the so-called permeability-selectivity trade-off (*11*–*13*). The prospect of bypassing the permeability-selectivity trade-off has led to extensive research in molecular sieving materials, such as carbon nanotubes and two-dimensional materials, as ion-selective membranes (*10*, *14*). Comparatively, much less attention has been given to tuning the coordinative interactions between a species of interest and membrane matrix—one key feature that purportedly imparts biological membranes with their remarkable selectivity (*15*, *16*).

The structure and mechanisms of biological channels suggest that tailoring interactions between a desired species and channel may lend greater selectivity, but few studies have investigated this selectivity mechanism in polymeric membranes. Some of these studies suggest that counterions that strongly bind to the charged functional groups of the polymer have lower permeability (*16*–*19*), which has led to development of adsorptive membranes requiring chemically induced regeneration to recover target species (*20*). Other reports claim that coordinative interactions promote higher permeability, or continuous removal without regeneration, of the stronger binding species (*21*–*23*). These inconsistencies may stem from a trade-off that exists between partitioning and diffusion; that is, more partitioning of a into a membrane is often accompanied by lower diffusivity of that species within the membrane (*16*, *24*). Mechanistic insights are needed to resolve how ion permeability and selectivity are affected by interactions with fixed, high-affinity binding sites. Such knowledge may uncover guidelines for designing membranes that couple high permeability and selectivity for continuous removal of high-value resources from water.

Here, we demonstrate how cation permeability and selectivity are affected by coordinative interactions with a polymer membrane. Our analysis focuses on transport of similar metal cations through polyelectrolyte multilayer membranes with iminodiacetate (IDA) functional groups, owing to their strong coordinative interactions

[1]Department of Chemical and Environmental Engineering, Yale University, New Haven, CT 06520-8286, USA. [2]Nanosystems Engineering Research Center for Nanotechnology-Enabled Water Treatment (NEWT), 6100 Main Street, MS 6398, Houston, TX 77005, USA. [3]Department of Civil and Environmental Engineering, Rice University, 6100 Main Street, Houston, TX 77005, USA. [4]Department of Materials Science and Nano Engineering, Rice University, 6100 Main Street, Houston, TX 77005, USA. [5]Department of Chemical and Biomolecular Engineering, Materials Science and NanoEngineering, Rice University, Houston, TX 77005, USA. [6]Key Laboratory of New Membrane Materials, Ministry of Industry and Information Technology; School of Environmental and Biological Engineering, Nanjing University of Science and Technology, Nanjing 210094, China.
*Corresponding author. Email: menachem.elimelech@yale.edu

(*21*, *25*, *26*). Results demonstrate that metal ions with higher binding energy to IDA groups more selectively pass through the membrane in multisalt solutions than in single-salt solutions, whereas the permeability of weaker binding species is markedly reduced because they are less likely to bind with IDA moieties. High selectivities are attained with ultrathin membranes, especially compared to polymer layers approaching the thickness of ion-exchange membranes, because the flux of the stronger binding species is thickness dependent and the permeability of the weaker binding species is thickness independent. Our findings show that with appropriate membrane design, including tailoring interactions between species of interest and an ultrathin selective layer, high precision and continuous ion-separation processes may be possible with polymeric membranes.

RESULTS

Ion transport with high binding energy

We prepared polyelectrolyte multilayer membranes with IDA groups to evaluate permeability and selectivity of divalent cations, which have strong interactions with the membrane. Membranes were fabricated with poly[(*N*,*N*-dicarboxymethyl)allylamine] (PDCMAA), which contains IDA groups, and poly(allylamine hydrochloride) (PAH), which contains primary amino groups. PDCMAA was synthesized via carboxymethylation of PAH, as reported previously (*25*, *27*), and both polymer structures were verified using proton nuclear magnetic resonance spectroscopy (fig. S1). Subsequently, we followed established procedures to produce $(PDCMAA/PAH)_n$ films of n bilayers (n = 2.5 to 11.5) on anodic aluminum oxide (AAO) substrates of 20- to 30-nm pores by alternating the deposition of partially anionic PDCMAA and cationic PAH (table S1 and fig. S2) (*21*, *25*). The surface modification of the AAO supports was confirmed via attenuated total reflectance Fourier transform infrared spectroscopy, and Cu^{2+} binding to the membrane was observed with scanning electron microscopy equipped with energy-dispersive x-ray spectroscopy (figs. S3 and S4).

Before experiments, we selected five divalent cations with extremely similar ionic radii and hydration enthalpies but disparate binding constants to IDA (log$K$) (Fig. 1A and table S2) (*28*–*30*). Similar divalent cations were tested to minimize differences in ionic size and charge, thereby isolating the relationship between chemical affinity and permeability to the degree possible. We then performed density functional theory (DFT) calculations to determine the binding structure and energy of these selected divalent metals to IDA groups, which were modeled as one monomer of dicarboxymethyl allylamine. Two coordination structures minimize binding energies of divalent species to IDA: one metal bound per IDA group and one metal bound per carboxylate group. The larger binding energies of the former structure suggest that one metal per IDA group is the predominant binding arrangement (Fig. 1B, figs. S5 and S6, and section S2.1). With this arrangement, Mg^{2+} has the lowest binding

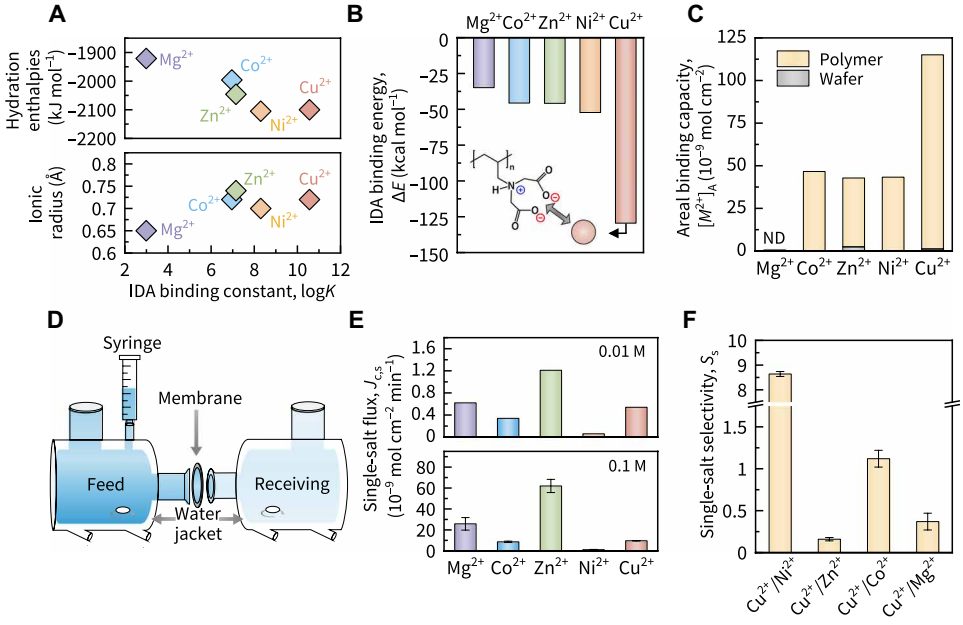

Fig. 1. Transport of similar divalent cations through polyelectrolyte multilayer membranes with iminodiacetate groups. (**A**) Hydration enthalpies (top) and ionic radii (bottom) of the selected divalent cations with similar sizes but varying binding constants to IDA, log$K$ (*28*–*30*). (**B**) Binding energy of divalent cations to monomeric dicarboxymethyl allylamine, which contains IDA, as determined by DFT calculations. (**C**) Cation binding capacity of $(PDCMAA/PAH)_{7.5}$ membranes per unit area of polymer. Films were fabricated on silicon wafers; immersed in 1 mM $CuCl_2$, $NiCl_2$, $ZnCl_2$, $CoCl_2$, or $MgCl_2$ (pH 3.6); and then eluted with 20 mM EDTA (pH 7). Yellow bars show the binding capacity to the polymer film, and gray bars show the binding capacity attributed to the silicon wafer (control). ND, no detection. (**D**) Schematic of the custom-built apparatus used for evaluating salt transport across $(PDCMAA/PAH)_n$ films on anodic AAO substrates. A 1.77-cm^2 membrane was mounted between feed and receiving chambers, which were temperature-controlled via a water jacket. Volume of the feed chamber was monitored by a calibrated syringe to determine water flux. (**E**) Cation flux through $(PDCMAA/PAH)_{3.5}$ membranes with single-salt feed compositions, $J_{c,s}$. Feed solutions contained 0.01 M (top) or 0.1 M (bottom) $CuCl_2$, $NiCl_2$, $ZnCl_2$, $CoCl_2$, or $MgCl_2$ (pH 3.6). (**F**) Single-salt selectivity between Cu^{2+} and other divalent cations with $(PDCMAA/PAH)_{3.5}$ membranes. Single-salt selectivity, S_s, was calculated using Eq. 5 with ion fluxes from 0.1 M experiments in (E). Experiments were conducted with deionized (DI) water as the receiving solution and temperature of 25° ± 0.1°C. All error bars represent one SD of three independent samples.

energy (−34.9 kcal mol^{-1}) and Cu^{2+} has the highest binding energy (−130 kcal mol^{-1}) of the cations selected (Fig. 1B). The binding energies for this structure are in agreement with the Irving-Williams order and experimental binding constants from literature (*28*, *31*).

We subsequently investigated how these theoretical binding energies ($Cu^{2+} > Ni^{2+} > Zn^{2+} > Co^{2+} > Mg^{2+}$) affect metal binding to the polymer membrane. We bound and eluted metal ions from the multilayer film, upon which metal uptake was quantified using inductively coupled plasma mass spectroscopy (ICP-MS). The areal and volumetric binding capacity of the polyelectrolyte multilayer membranes for divalent cations corresponds relatively well with the theoretical binding energies derived from DFT (Fig. 1C and fig. S7). Polymer films comprising $(PDCMAA/PAH)_{7.5}$ have the highest areal binding capacity for Cu^{2+}, whereas Mg^{2+} was not detected because its interactions were weak or easily reversed after rinsing with water. The relationship between the binding energy and metal uptake of the membrane provides evidence that ion-membrane interactions affect the binding selectivity of the polymer films.

Polyelectrolyte multilayer membranes were then tested in a diffusion cell with mixing and a temperature-controlled water jacket (Fig. 1D and fig. S8). Experiments were performed with $(PDCMAA/PAH)_{3.5}$ membranes, which comprise three bilayers of PDCMAA/PAH and a PDCMAA terminating layer (seven total polymer layers). We first investigated whether IDA groups within the membrane, not amino groups of PAH, were the principal binding sites for transport of divalent cations. Increasing solution pH could allow Cu^{2+} to readily compete with protons for the lone pair of $-NH_2$ ($pK_a \approx 9.3$, where K_a is the acid dissociation constant), which would provide more binding sites for transport and increase Cu^{2+} flux (*28*, *32*). Instead, increasing the feed and receiving compartment pH from 2.5 to 3.6 slightly reduced Cu^{2+} flux (fig. S9). The lower Cu^{2+} flux at pH 3.6 could be explained by altered binding strength to IDA groups, which could have counterbalanced or concealed effects of $-NH_2$ binding on flux. Therefore, these data do not eliminate do not eliminate the possibility of $-NH_2$ binding but also do not provide evidence of its occurrence. To more conclusively rule out $-NH_2$ binding, we performed DFT calculations and found that the binding energy to $-NH_2$ is more than 70 kcal mol^{-1} higher for H^+ than for the selected divalent cations (fig. S10), which reinforces that $(PDCMAA/PAH)_n$ membranes facilitate transport of divalent cations via IDA sites (section S2.2).

Diffusive fluxes were measured with single-salt feed solutions of the selected divalent cations to probe whether strong ion-IDA binding significantly hinders cation transport (Fig. 1E). Reverse water fluxes were reasonably similar across experiments ($J_w \approx 2.54 \pm 0.33$ L m^{-2} hour^{-1}), indicating similar osmotic pressures and concentration differences (i.e., driving force) for salt permeability (fig. S11). Nevertheless, we did not observe a correlation between the binding energy and single-salt cation flux, $J_{c,s}$. The strongest binding species Cu^{2+} exhibited a 11.2 ± 0.86% higher flux than a weaker binding species Co^{2+} (*29*). More flux variability was observed between other species, leading to single-salt selectivities (S_s) for Cu^{2+} over weaker binding species (Ni^{2+}, Zn^{2+}, Co^{2+}, or Mg^{2+}) ranging from approximately 0.1 to 9 (Fig. 1F). These moderate selectivities do not strongly correlate with any single cation property (e.g., ion size or diffusivity) but may stem from collective differences between species (table S2) (*29*, *30*, *33*). In the following section, we further investigate binding effects on cation permeability by analytically controlling for these property differences in multisalt experiments.

Binding energy differences govern transport

Diffusion experiments were performed with $(PDCMAA/PAH)_{3.5}$ membranes in multicomponent feed solutions containing equimolar concentrations of the strongest binding species (Cu^{2+}) and one weaker binding species (Ni^{2+}, Zn^{2+}, Co^{2+}, or Mg^{2+}). Like single-salt experiments, water fluxes verify osmotic pressures and concentration differences were about equal in multisalt experiments ($J_w \approx 3.91 \pm 0.34$ L m^{-2} hour^{-1}) (fig. S11). Multisalt fluxes ($J_{c,m}$) were approximately constant for Cu^{2+} at (17.8 ± 1.06) × 10^{-9} mol cm^{-2} min^{-1}, which was greater than fluxes of all weaker binding species, except Zn^{2+} (Fig. 2A). The multisalt selectivities for Cu^{2+} (S_m) ranged from 0.84 ± 0.13 for Cu^{2+}/Zn^{2+} to 52.1 ± 34.1 for Cu^{2+}/Mg^{2+} (Fig. 2B). We emphasize that these high selectivities between such similar ions (specifically Cu^{2+}/Mg^{2+}, Cu^{2+}/Co^{2+}, and Cu^{2+}/Ni^{2+}) are uncharacteristic of polymeric membranes. Notably, the hydrated radii of these species differ by only 0.09 Å (Cu^{2+}/Mg^{2+}), 0.04 Å (Cu^{2+}/Co^{2+}), and 0.15 Å (Cu^{2+}/Ni^{2+}) (*29*). Only molecular recognition through coordination chemistry, which occurs via a facilitated transport mechanism, can explain such precise separations (fig. S12 and section S2.4) (*21*).

The high selectivities originate from reduced fluxes of weaker binding species in the presence of a stronger binding species (Cu^{2+}). To determine this, we normalized the cation fluxes in multisalt solutions to those observed in single-salt solutions (i.e., $J_{c,m}/J_{c,s}$), where feed compartments contained equal concentrations of the weaker binding cation (0.1 M) with or without 0.1 M $CuCl_2$. We observed an increase in Cu^{2+} fluxes in multisalt experiments by 184 ± 68.9% (Fig. 2C), which is attributable to the larger Cl^- concentration when multiple salts are present. More specifically, a greater Cl^- flux established a membrane potential that accelerated Cu^{2+} (and other cations) to maintain charge neutrality (*34*, *35*). Conversely, the normalized cation flux for a weaker binding species decreased roughly in proportion to its difference in IDA binding energy or binding constant with Cu^{2+} (Fig. 2C and fig. S13). The permeability of weaker binding species diminished in multisalt solutions because of lower binding energy, or lower probability of binding, with IDA moieties compared to Cu^{2+}. Reduced flux of weaker binding species persisted even without $CuCl_2$ in the feed solution, as long as IDA sites within the membrane were preloaded with Cu^{2+} (fig. S14) (*21*).

This competitive binding mechanism may appear to suggest that weaker binding species always had lower fluxes than stronger binding Cu^{2+}, although this was not the case. Rather, it suggests that passage of weaker binding species decreased in the multisalt solution compared to the single-salt solution. For example, the flux of Zn^{2+} was significantly higher than Cu^{2+} in single-salt experiments (Fig. 1E). When the passage of Zn^{2+} decreased in the multisalt solution owing to its lower binding energy than Cu^{2+} (Fig. 2C), the flux reduction was not large enough to favor Cu^{2+} passage over Zn^{2+}. We also note that flux reductions of weaker binding species, like Zn^{2+}, would likely be larger without the additional driving force from Cl^- transport imposed by the experimental design.

Competition for IDA sites considerably reduced the permeability of the weaker binding species, which, in turn, produced higher selectivity for a stronger binding species in multisalt solutions than single-salt solutions. From normalizing the multisalt selectivity to the single-salt selectivity (i.e., S_m/S_s), we can estimate the improvement in cation selectivity that is attributable to competitive binding to IDA (Fig. 2D and fig. S13). Weak interactions with amino groups of PAH, if present, could promote a similar selectivity trend (figs. S15

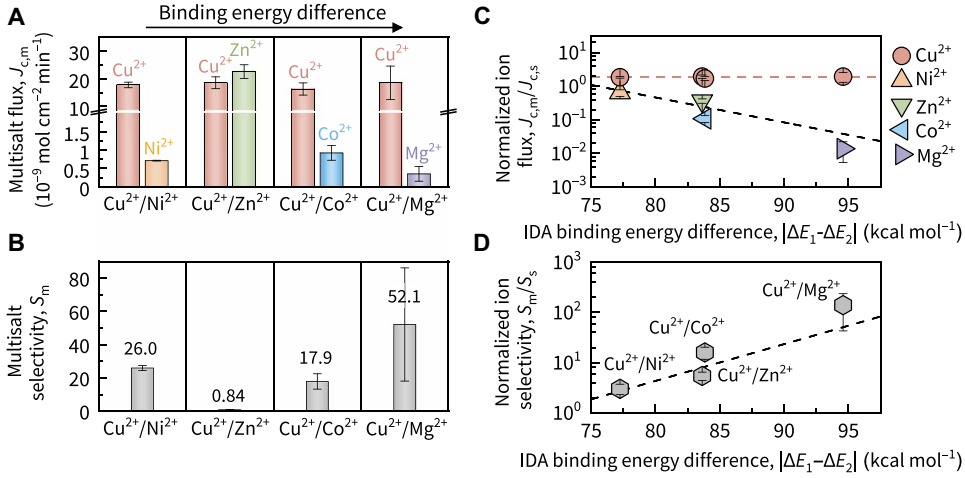

Fig. 2. Selectivity between similar divalent cations via tailored ion-membrane interactions. (**A**) Cation flux with multisalt feed compositions, $J_{c,m}$. Feed solutions contained 0.1 M $CuCl_2$ and 0.1 M of one of the following salts: $NiCl_2$, $ZnCl_2$, $CoCl_2$, or $MgCl_2$ (pH 3.6). (**B**) Cu^{2+} selectivity over similar cations (Ni^{2+}, Zn^{2+}, Co^{2+}, or Mg^{2+}) in multisalt feed solutions, S_m. Results were calculated using Eq. 5 from fluxes reported in (A). (**C**) Relationship between ion binding energy to IDA and normalized ion flux. The two species at each *x* coordinate represent the two cations present in the multisalt feed solution. The IDA binding energy difference was calculated as the binding energy of the strong binding species (Cu^{2+}) minus the binding energy of the weaker binding species (Ni^{2+}, Zn^{2+}, Co^{2+}, or Mg^{2+}) in the multisalt feed solution. Normalized ion flux was defined as $J_{c,m}/J_{c,s}$, which was calculated from data in (A) and single-salt flux, $J_{c,s}$, in Fig. 1E (0.1 M). (**D**) Relationship between ion binding energy to IDA and normalized Cu^{2+} selectivity. Normalized Cu^{2+} selectivity was defined as S_m/S_s, which was calculated from data in (B) and single-salt selectivity, S_s, reported in Fig. 1F (0.1 M). All experiments were conducted with $(PDCMAA/PAH)_{3.5}$ membranes, DI water as the receiving solution, and temperature of 25° ± 0.1°C. All error bars represent one SD of three independent samples.

and S16), but evidence suggests that binding does not occur between cations and amino groups of PAH (see the previous section). In summary, our findings highlight that increasing the ion-membrane binding energy of a target ion relative to an interfering species substantially enhances the selectivity for the target ion by excluding weaker binding species. These results have meaningful implications for the design of ion-selective membranes.

Selectivity is dependent upon membrane thickness

The mechanisms by which coordinative interactions influence transport indicate that tailoring ion-membrane binding energies is a promising method for increasing ion selectivity. These results, however, were collected for polymer films with dry thicknesses (δ_d) of 35.1 ± 3.51 nm, which may not translate to other ion-selective membranes that are considerably thicker, such as ion-exchange membranes. Understanding how competition for ion-exchange sites affects performance in thicker membranes may uncover previously unidentified mechanistic insights about ion transport that can guide ion-selective membrane design.

We prepared $(PDCMAA/PAH)_n$ films of varying thicknesses by increasing the number of polymer bilayers (n = 2.5 to 11.5) applied to structural support layers. To measure the film depth, we used a step-height method in profilometry with polymer films fabricated on atomically smooth silicon wafers (*36*). Measured step heights on silicon wafers are estimates of film thicknesses on AAO substrates, given the differences in substrate surface chemistry and physical structure. For $(PDCMAA/PAH)_{3.5}$ films, the film thickness on a silicon wafer (35.1 ± 3.51 nm) agrees reasonably well with the measured thickness on an AAO substrate (47.0 ± 6.25 nm), where the latter was obtained from a scanning electron microscopy image (fig. S17). The step heights of the dry films, which ranged from 13.8 ± 3.07 nm (n = 2.5) to 930 ± 140 nm (n = 11.5) (Fig. 3A), grew with the number of applied bilayers (fig. S18). The fabricated films are thinner than typical ion-exchange membranes (δ_d > 20 μm) but are nonetheless adequate for studying membrane structure–property–performance relationships (*37*).

Selectivity of nonporous polymeric membranes is typically considered to be independent of membrane thickness, as fluxes of all species scale nearly proportionately with reducing thickness (*34*, *38*). This behavior follows the solution-diffusion model, which states that $J_c = P_c\Delta C_m/\delta$, where J_c is the measured cation flux, P_c is the thickness-independent cation permeability, ΔC_m is the solute concentration difference across the membrane, and δ is the effective film thickness (*39*). To test the relationship between film thickness and selectivity, we performed experiments with feed solutions of 0.1 M $CuCl_2$ or $CoCl_2$ and a sucrose receiving solution of equal osmolarity. A sucrose receiving solution eliminated reverse water flux and concentration polarization to allow direct comparison of cation permeabilities for membranes of varying thicknesses.

In single-salt diffusion experiments, the Cu^{2+} and Co^{2+} fluxes for $(PDCMAA/PAH)_{3.5}$ films increased by 60 ± 6% and 24 ± 5%, respectively, by eliminating water transport with a sucrose receiving solution. We confirmed single-salt Cu^{2+} and Co^{2+} fluxes to be inversely proportional to dry thickness of $(PDCMAA/PAH)_n$ films, although this relationship appears to subside for the thickest films (Fig. 3B). After normalizing cation fluxes by film thickness, we observed an increase in Cu^{2+} and Co^{2+} permeability with growing thickness, whereas the phenomenological solution-diffusion model considers permeability to be independent of thickness (Fig. 3C). This deviation could arise from changes in intrinsic film properties, limitations of the methods for estimating thickness, or imperfect assumptions in the model (e.g., P_c is a material constant) (*39*).

Analysis of the effect of membrane thickness on ion transport requires that intrinsic film properties be well preserved with

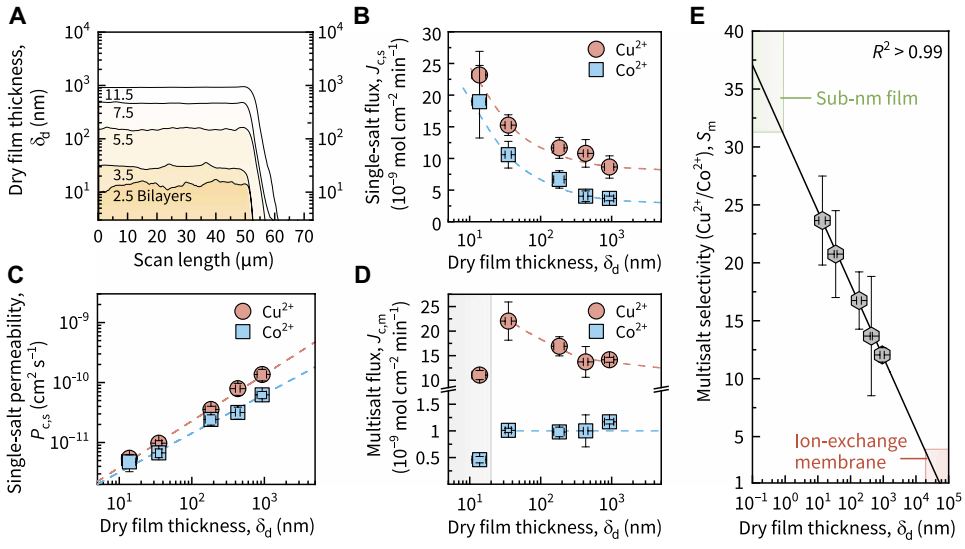

Fig. 3. Projected selectivity of subnanometer films and ion-exchange membranes. (**A**) Cross-sectional profiles from profilometry used to determine dry $(PDCMAA/PAH)_n$ membrane thickness ($n = 2.5$ to 11.5). Films were fabricated on silicon wafers, dried in vacuum, and scratched with a needle before step-height analysis. (**B**) Cation flux with single-salt feed compositions. Feed solutions contained 0.1 M $CuCl_2$ or $CoCl_2$ (pH 3.6) and receiving solutions contained 0.251 M sucrose in (B) and (C). (**C**) Cation permeability through $(PDCMAA/PAH)_n$ films with single-salt feed compositions. (**D**) Cation flux with multisalt feed compositions. With decreasing film thickness, Cu^{2+} flux increased and Co^{2+} flux remained relatively constant, except for $(PDCMAA/PAH)_{2.5}$ films (gray region). Feed solutions contained 0.1 M $CuCl_2$ and 0.1 M $CoCl_2$ (pH 3.6) and receiving solutions contained 0.495 M sucrose, respectively, in (D) and (E). (**E**) Cu^{2+}/Co^{2+} selectivity, S_m, with multisalt feed solutions as a function of film thickness. Linear extrapolation suggests $S_m > 30$ for subnanometer films (green region) and $S_m < 5$ for film thicknesses typical for ion-exchange membranes (red region). Results were calculated using Eq. 5 from fluxes reported in (D). All experiments were conducted with $(PDCMAA/PAH)_n$ membranes at a temperature of 25° ± 0.1°C. All error bars represent one SD of three independent samples.

additional film growth. Polymer films fabricated by sequential layer-by-layer assembly were expected to maintain reasonably similar properties for thicker films, as they have been used previously under this premise (*40*). We investigated whether intrinsic film properties remained constant by comparing the slopes of Cu^{2+} and Co^{2+} permeabilities with varying film thicknesses (Fig. 3C). We found that the permeability of Cu^{2+} increased slightly more than Co^{2+} with increasing number of polymer bilayers. The ratios of Cu^{2+} and Co^{2+} permeabilities, or single-salt selectivity, as a function of film thickness provide additional insight into intrinsic film properties (fig. S19). Thicker $(PDCMAA/PAH)_n$ films became slightly more selective for Cu^{2+}, with Cu^{2+}/Co^{2+} permeability ratios ranging from 1.22 ± 0.42 ($n = 2.5$) to 2.67 ± 0.77 ($n = 7.5$). Results indicate that physical and chemical properties of the film (e.g., pore structure or functional group density) slightly change with increasing thickness to become more selective toward Cu^{2+}. In comparison to reported multisalt selectivities (Fig. 2B), these changes in film properties are small, but nonetheless present error when comparing transport properties of membranes with different thickness.

With this limitation in mind, we performed diffusion experiments with a mixture of 0.1 M $CuCl_2$ and 0.1 M $CoCl_2$ in the feed compartment (Fig. 3D). Like single-salt experiments, the Cu^{2+} flux increased at smaller film thicknesses. Flux of the weaker binding species Co^{2+}, on the other hand, showed no statistically significant difference for $(PDCMAA/PAH)_n$ films between 35.1 ± 3.51 nm ($n = 3.5$) and 930 ± 140 nm ($n = 11.5$) in thickness [one-way analysis of variance (ANOVA), $P = 0.49$]. Flux trends broke down as the $(PDCMAA/PAH)_n$ film thickness reduced below the pore sizes of the AAO support (20 to 30 nm) at $n = 2.5$ (13.8 ± 3.07 nm), as shown in the gray region of Fig. 3D. Previous reports have established that flux does not increase when polymer-selective layers become extremely thin, if the solute diffusion length increases (*41*, *42*). This behavior can occur when solutes must laterally diffuse through an ultrathin polymer film to reach pores of the support layer (*41*, *42*). Lateral diffusion could explain the anomalous multisalt fluxes for $(PDCMAA/PAH)_{2.5}$ films, although it is unclear why this behavior is not present in single-salt experiments (Fig. 3B).

Incorporating coordination chemistry into a polymeric membrane created a thickness-independent Co^{2+} flux, which, in turn, yielded a Cu^{2+}/Co^{2+} selectivity strongly contingent on film thickness ($R^2 > 0.99$) (Fig. 3E). The highest selectivities were attained for thinner membranes, including $n = 2.5$ ($S_m = 23.6 \pm 3.84$), which is primarily attributed to lower resistance to Cu^{2+} flux. From the strong thickness-selectivity relationship, we project theoretical selectivity values for subnanometer films and 20-μm films, where the former is similar to the K^+ channel (1.2 nm) and the latter is representative of a thin ion-exchange membrane. Notably, the slope of the line suggests that Cu^{2+}/Co^{2+} selectivities exceeding 30 are possible for subnanometer films. In contrast, Cu^{2+}/Co^{2+} selectivities less than 5 are expected for thicknesses typical of ion-exchange membranes.

These projections suggest that significantly higher selectivities are possible with thin layers of binding sites, although they ignore possible constraints in creating a subnanometer film via polyelectrolyte layer-by-layer assembly. Projections also assume that intrinsic membrane properties remained similar for all films. Evidence suggests, however, that film properties changed to produce higher single-salt selectivity for Cu^{2+} with increasing film thickness (Fig. 3C and fig. S19). Critically, this behavior indicates that multisalt selectivity at larger film thicknesses may be overestimated. Therefore, we expect that removing film nonuniformities

would impose a steeper, not gentler, slope in the thickness-selectivity relationship.

The thickness-dependent membrane performance can be directly attributed to effects from competitive binding to IDA groups. Cation transport through the film is governed by a rate-limiting step, which for polymeric membranes is typically considered diffusion within the membrane (fig. S20) (*39*). A diffusion-limited process is dependent upon membrane thickness (*34*, *39*), bearing resemblance to the flux behavior of Cu^{2+} in Fig. 3D. Alternative rate-determining steps are cations diffusing from the bulk solution into the membrane or cations reacting with IDA groups, which are interfacial processes independent of membrane thickness (*34*, *43*). Therefore, data support that the rate-limiting step for Co^{2+} transport in single-salt solutions is diffusion through the membrane (Fig. 3B) and in multisalt solutions is diffusion through the water-membrane interface or reacting with IDA groups (Fig. 3D and fig. S20). Mechanistic understanding of competitive binding supports this claim: In multisalt solutions, a weaker binding species (Co^{2+}) is less likely to compete for IDA sites at the water-membrane interface, which considerably hinders its transport rate.

DISCUSSION

Most attempts to introduce coordination chemistry into polymeric membranes have yet to significantly improve selectivity between ions of similar size and charge. Our work demonstrates two methods for increasing selectivity for a specific ion: (i) increasing the binding energy of the target ion relative to an interfering species and (ii) reducing membrane thickness. Specifically, we show that competitive binding effects can significantly hinder weaker binding species from partitioning into the membrane, which produces selectivity that is strongly determined by membrane thickness. The slope of the thickness-selectivity relationship is likely contingent upon membrane-specific properties or, more explicitly, the solubility of the weaker binding species and the diffusivity of the strong binding species in the membrane. For the polyelectrolyte multilayer membranes studied here, we show that reducing membrane thickness from 20 μm to 1 nm increases the projected Cu^{2+}/Co^{2+} selectivity from less than 5 to more than 30.

While we expect that the conceptual findings translate to other membrane chemistries, there are some notable exceptions to when these methods may be effectively applied. For example, membranes that irreversibly bind target species are unlikely to exhibit selectivity for that species, perhaps unless an external driving force is applied to overcome the desorption energy barrier. Moreover, membranes with low sorption selectivity, which are specifically unable to substantially hinder a weaker binding species from entering the membrane, will not have improved selectivity with smaller thicknesses when the rate-determining transport step of a weaker binding species is diffusion through the membrane. Reducing sorption of weaker binding species may require increasing membrane binding strength for the target ion, decreasing pore size, or increasing binding site density of the membrane. Some of these factors may explain why, to our knowledge, there are no reports of conventional ion-exchange membranes with selectivity that is strongly dependent upon thickness, although this may be the subject of future investigation.

Tailoring ion-polymer interactions and membrane thickness could facilitate separations that were previously considered unfeasible for polymeric materials. If highly selective membranes could be incorporated into a high-throughput process (e.g., electrodialysis or nanofiltration), targeted removal and recovery of valuable metals from concentrated sources with polymeric membranes may become conceivable. Such a membrane process would continuously remove target species without any requirement for chemical regeneration, which provides a noteworthy advantage over adsorption processes. A limitation, however, is that a pre- or postseparation step would be necessary to isolate divalent cations from monovalent cations, as membranes with coordination chemistry are unlikely to adequately reject small, monovalent species while removing divalent species.

Fabrication techniques are also needed to form ultrathin polymer membranes with superior stability and robustness than ionically cross-linked polymer multilayers on AAO substrates. Thin-film deposition techniques like atomic or molecular layer deposition may provide the molecular-level control necessary to create supported films of a desired thickness and chemistry (*44*, *45*). Alternatively, functionalizing only the membrane surface with binding sites could enhance partitioning selectivity without markedly hindering diffusion (*35*). Porous nanomaterials, such as carbon nanotubes and covalent organic frameworks, with functionalized pore entrances may satisfy these criteria (*46*, *47*), although fabricating a defect-free membrane with these materials presents an additional challenge. Ideally, a successful fabrication technique would provide access to a range of membrane chemistries that would open applicability to other commercially relevant separations. Lithium recovery from brines, uranium recovery from seawater, and nitrate from wastewater are among the separations that could be possible with highly selective membranes.

MATERIALS AND METHODS

Membrane fabrication

PDCMAA was synthesized and characterized as described in section S1.2 (*25*, *27*). Polyelectrolyte films were formed on AAO substrates with 20- to 30-nm pore size via dip coating. Before fabrication, polymer deposition solutions were prepared with 0.01 M polymer (calculated with respect to the repeating unit) and 0.5 M background ionic strength (NaCl). We note that polymer concentrations are likely overestimated because of adsorbed Na^+ and water to the PDCMAA. Polymer solutions were adjusted to pH 3.0 to protonate PAH ($pK_a \approx 9.3$) and partially protonate carboxylate groups of PDCMAA ($pK_a \approx 1.8, 2.6$) (*28*, *32*). The solution ionic strength and low charge density of PDCMAA impart the membrane with high metal binding capacity, which may be attributed to the film thickness and fewer ionic bonds between IDA groups of PDCMAA and amino groups of PAH (*21*, *25*).

During layer-by-layer assembly, an AAO substrate was sandwiched between rubber gaskets. The gaskets were then secured between a glass plate and a hollow, polytetrafluoroethylene frame using metal clips. One side of the pristine AAO substrate was then immersed and shaken (60 rpm) in polyanion (PDCMAA) solution for 5 min, followed by continuously rinsing with deionized (DI) water for 1 min. Subsequently, membranes were immersed and shaken (60 rpm) in polycation (PAH) solution for 5 min and rinsed for 1 min with DI water to remove any loosely adsorbed polymer. This process produced one polyelectrolyte bilayer and was repeated to produce $(PDCMAA/PAH)_n$ films of n bilayers (n = 2.5 to 11.5). Last, membranes were thoroughly rinsed and stored in DI water until use.

Membrane thickness characterization

Profilometry was performed using a DektakXT stylus profilometer (Bruker) to analyze dry film thickness on silicon wafers. Before polymer deposition, substrates were cleaned for 10 min in an ultraviolet/ozone cleaner (BioForce Nanosciences ProCleaner Plus), rinsed with water, dried with N_2 gas, and stored in ambient air. Wafer surfaces were first coated with a monolayer of amine precursor by immersion in 5 mM cystamine dihydrochloride for 1 hour (*48*). After rinsing with water, polyelectrolyte multilayers were fabricated on silicon wafers with otherwise identical methods as described for AAO supports. Samples were dried overnight in ambient air and then carefully sliced with a metal needle without damaging the wafer.

Profilometry was then used to measure dry film thickness (δ_d) with a tip radius of 12.5 μm, a stylus force of 5 mg, and a scanning time of 15 s. A stylus scan range of 65.5 μm was used for films less than 500 nm (*z* resolution ≈ 1 nm), and a stylus scan range of 524 μm was used for films greater than 500 nm (*z* resolution ≈ 8 nm). Step heights were calculated by averaging the film thickness over a >250-μm bandwidth perpendicular to the edge of the polymer film. Step heights were measured at four randomly selected positions along the film edge. Additional membrane characterization is described in section S1.3.

DFT simulations

DFT calculations were performed using Gaussian 16 package (*49*) to determine binding energies of a set of ions (Cu^{2+}, Ni^{2+}, Zn^{2+}, Co^{2+}, and Mg^{2+}) to IDA and amine functional groups, which were modeled as one monomer of dicarboxymethyl allylamine (negatively charged) and allylamine (neutral), respectively. These models assume that one monomer binds to one metal ion, although two monomers could bind with a metal ion and increase binding strength (*28*). The nitrogen atom and carboxylate groups in dicarboxymethyl allylamine were assumed to be protonated and deprotonated, respectively, based on the pH of the experimental feed solution (pH 3.6). Protonation of the nitrogen atom of dicarboxymethyl allylamine was examined via DFT calculations when Cu^{2+} is bound to IDA, using methods described below. The H^+ binding energy to the nitrogen atom was −129 kcal mol^{-1}, which confirms protonation after complexation of Cu^{2+} (or other weakly bound cations) with IDA. The H^+ binding energy was computed to be −199 kcal mol^{-1} in the absence of divalent cations.

Geometry optimizations using the Berny algorithm were performed for each functional group and ion-functional group complex to determine the most favorable binding configuration (*50*). The binding/interaction energy between each cation, *c*, and a functional group, *f*, was then computed as

$$\Delta E = E_{c,f} - E_f - E_c \quad (1)$$

where *E* is the zero-point vibrational energy-corrected electronic total energy of each system,Δ*E* is the total interaction energy, $E_{c,f}$ is the energy of the ion-functional group complex, E_f is the energy of the isolated functional group, and E_c is the energy of the isolated ion. The interaction energy between an ion-functional group complex and an unbound second ion was calculated as

$$\Delta E = E_{c_2,c_1,f} - E_{c_1,f} - E_{c_2} \quad (2)$$

where $E_{c2,c1,f}$ is the energy of the unbound second ion and the ion-functional group complex together, $E_{c1,f}$ is the energy of the ion-functional group complex, and E_{c2} is the energy of the unbound second ion. Calculations were performed in vacuum or implicit water solvent using the conductor-like polarizable continuum model to account for the presence of surrounding water molecules (*51*, *52*). The B3LYP functional with a mixed basis set was used to perform the DFT calculations. The aug-pc-1 basis set was used for Cu^{2+}, Ni^{2+}, Zn^{2+}, and Co^{2+} ions, and the 6-31+G* basis set was used for all other atoms. These results were compared with using the LANL2DZ basis set for Cu^{2+}, Ni^{2+}, Zn^{2+}, and Co^{2+} species, which yielded similar results but with a slight dissimilarity for Zn^{2+} from the well-established Irving-Williams order and literature binding constants (fig. S21) (*28*, *31*, *53*).

Diffusion cell measurements

A custom-made diffusion cell with two 60-ml chambers and a water jacket was used for membrane performance testing. A membrane (1.77 cm^2) was mounted between the two chambers with its active layer side toward the feed solution. The water jacket was maintained at 25° ± 0.1°C with a cooling/heating recirculator (Cole Palmer Polystat) to control internal solution temperature. Approximately 15 min was given for the cooling/heating recirculator to stabilize the diffusion cell temperature before testing. Feed solutions contained 0.01 or 0.1 M of one or more salts ($CuCl_2$, $NiCl_2$, $ZnCl_2$, $CoCl_2$, or $MgCl_2$), and the receiving solution contained DI water, unless otherwise specified. Feed solutions were adjusted to pH 3.6 using HCl to avoid hydrolysis of metals. When additional pH adjustments were necessary, we adjusted both the feed and receiving compartment pH using HCl so that Cl^- concentration differences and osmotic pressures were equal across experiments. Each chamber was continuously stirred with a stir bar.

The change in feed volume (Δ*V*) was monitored using a calibrated syringe to calculate reverse water flux (J_w) using

$$J_w = \frac{\Delta V}{A\Delta t} \quad (3)$$

where *A* is the membrane area (1.77 cm^2) and Δ*t* is the permeation time (hours). Over the testing period, the concentration change in the receiving compartment was negligible compared to the feed concentration such that the concentration difference remained approximately constant. Every 1 hour for a total of 7 hours, 0.5 ml from the receiving chamber was taken and diluted 10-fold with 1% (v/v) HNO_3. Diluted samples were analyzed using ICP-MS (ELAN DRC-e, Perkin Elmer) to quantify concentrations of Cu^{2+}, Ni^{2+}, Zn^{2+}, Co^{2+}, and Mg^{2+}. Membrane cation flux (J_c) was then calculated via

$$J_c = \frac{C_r(V_r - \Delta V)}{A\Delta t} \quad (4)$$

where C_r is the solute concentration in the receiving chamber (mol $liter^{-1}$) and V_r is the initial volume of the receiving chamber (liters). Cation flux was calculated for single-salt solutions ($J_{c,s}$) and multi-salt solutions ($J_{c,m}$). Cation and water fluxes were consistent over the duration of experiments, suggesting negligible change in the driving force. Membrane selectivity, *S*, for the transport of one cation, *i*, over another cation, *j*, was calculated using

$$S = \frac{J_i/J_j}{C_i/C_j} \quad (5)$$

where J_i is the flux of component i (mol cm^{-2} min^{-1}) and C_i is the concentration of component i in the feed solution (mol liter^{-1}). Membrane selectivity was calculated when species were in independent single-salt feed solutions, referred to as single-salt selectivity (S_s), and when species were in the same feed solution, referred to as multisalt selectivity (S_m). The uncertainties in $J_{c,m}/J_{c,s}$, S_s, S_m, and S_m/S_s were determined with standard propagation of uncertainty methods. Error bars represent SDs from three fabricated membranes.

For testing membranes of different thicknesses, the receiving chamber contained sucrose (342.3 g mol^{-1}) to balance the osmolarity in the feed and receiving chambers. Osmotic pressures were calculated using the van 't Hoff equation, which takes osmotic coefficients into account (*54*). The receiving solution contained 0.251 and 0.495 M sucrose in the single- and multisalt experiments, respectively. The sucrose receiving solution may have also altered membrane properties compared to DI water, but we assume these changes to be similar for polymer films of different thickness. Permeabilities were calculated with respect to dry film thickness, which may have led to slightly underestimated values because these films slightly swell in water (~10%) (*25*).

To ensure that little to no sucrose crossover occurred, we performed diffusion experiments with DI water in the feed chamber and 0.495 M sucrose in the receiving chamber. We collected 0.5-ml feed samples every 1 hour for a total of 7 hours while testing a $(PDCMAA/PAH)_{2.5}$ membrane. Samples were diluted 30-fold, and the sucrose concentration was measured using a total organic carbon analyzer (TOC-VCSH, Shimadzu). For three independent experiments, we did not detect any sucrose in the feed compartment (<1 mg liter^{-1}) over the experimental duration, indicating that sucrose was mostly retained in the receiving compartment (fig. S22).

Binding capacity determination

Membrane binding capacity was determined for silicon wafers modified with cystamine dihydrochloride and $(PDCMAA/PAH)_{7.5}$ films using fabrication procedures described above. Larger film thicknesses (7.5 bilayers) were used to ensure detectable amounts of metals eluted from the membranes. Membranes were immersed for 14 days in 2 ml of 1 mM $CuCl_2$, $NiCl_2$, $ZnCl_2$, $CoCl_2$, or $MgCl_2$ (adjusted to pH 3.6 with HCl) at room temperature. Sorption solutions were exchanged multiple times because metal binding displaces protons from the film and slightly lowers solution pH. After rinsing with DI water for 1 min, metal ions were eluted by submerging the membrane in 10 ml of 20 mM EDTA (adjusted to pH 7.0 using NaOH), which has a much higher binding constant for metal ions than IDA (*28*). The amount of EDTA relative to IDA groups should have ensured uptake of all metal ions from the polymer film (*25*). After 7 days, a 0.5-ml aliquot was removed and diluted 10-fold with 1% (v/v) HNO_3. The metal concentration was determined using ICP-MS. The areal and volumetric binding capacity of the membrane, $[M^{2+}]_A$ and $[M^{2+}]_V$, were quantified using

$$[M^{2+}]_A = C_e\left(\frac{V_e}{A}\right) \quad (6)$$

$$[M^{2+}]_V = C_e\left(\frac{V_e}{A\delta_d}\right) \quad (7)$$

where C_e is the measured concentration of the desorption solution (mol liter^{-1}), V_e is the volume of the desorption solution (liters), and A is the projected surface area of the film (1.77 cm^2). Binding capacity of the $(PDCMAA/PAH)_{7.5}$ films was calculated by subtracting the binding capacity of control wafers that were modified with only cystamine dihydrochloride. If we assume that the $(PDCMAA/PAH)_{7.5}$ films have a density of 1 g cm^{-3}, contain 53% PDCMAA (47% PAH), and bind one metal ion per IDA group, the maximum areal binding capacity of the film is approximately 130×10^{-9} mol cm^{-2}. These films slightly swell in water (~10%) such that measured volumetric binding capacity may be overestimated (*25*).

SUPPLEMENTARY MATERIALS

Supplementary material for this article is available at https://science.org/doi/10.1126/sciadv.abm9436

REFERENCES AND NOTES

1. R. Epsztein, R. M. DuChanois, C. L. Ritt, A. Noy, M. Elimelech, Towards single-species selectivity of membranes with subnanometre pores. *Nat. Nanotechnol.* **15**, 426–436 (2020).
2. R. Sujanani, M. R. Landsman, S. Jiao, J. D. Moon, M. S. Shell, D. F. Lawler, L. E. Katz, B. D. Freeman, Designing solute-tailored selectivity in membranes: Perspectives for water reuse and resource recovery. *ACS Macro Lett.* **9**, 1709–1717 (2020).
3. M. A. Shannon, P. W. Bohn, M. Elimelech, J. G. Georgiadis, B. J. Mariñas, A. M. Mayes, Science and technology for water purification in the coming decades. *Nature* **452**, 301–310 (2008).
4. D. S. Sholl, R. P. Lively, Seven chemical separations to change the world. *Nature* **532**, 435–437 (2016).
5. International Energy Agency (IEA), *The Role of Critical Minerals in Clean Energy Transitions* (IEA Publications, 2021).
6. E. Gouaux, R. MacKinnon, Principles of selective ion transport in channels and pumps. *Science* **310**, 1461–1465 (2005).
7. Y. Zhou, J. H. Morais-Cabral, A. Kaufman, R. MacKinnon, Chemistry of ion coordination and hydration revealed by a K^+ channel–Fab complex at 2.0 Å resolution. *Nature* **414**, 43–48 (2001).
8. Y. Marcus, The thermodynamics of solvation of ions. Part 2.—The enthalpy of hydration at 298.15 K. *J. Chem. Soc. Faraday Trans. 1* **83**, 339–349 (1987).
9. D. A. Doyle, M. Cabral, R. A. Pfuetzner, A. Kuo, J. M. Gulbis, S. L. Cohen, B. T. Chait, R. MacKinnon, The structure of the potassium channel: Molecular basis of K^+ conduction and selectivity. *Science* **280**, 69–77 (1998).
10. R. M. DuChanois, C. J. Porter, C. Violet, R. Verduzco, M. Elimelech, Membrane materials for selective ion separations at the water–energy nexus. *Adv. Mater.* **33**, 2101312 (2021).
11. G. M. Geise, H. Bum, A. C. Sagle, B. D. Freeman, J. E. McGrath, Water permeability and water/salt selectivity tradeoff in polymers for desalination. *J. Membr. Sci.* **369**, 130–138 (2011).
12. L. M. Robeson, Correlation of separation factor versus permeability for polymeric membranes. *J. Membr. Sci.* **62**, 165–185 (1991).
13. G. M. Geise, M. A. Hickner, B. E. Logan, Ionic resistance and permselectivity tradeoffs in anion exchange membranes. *ACS Appl. Mater. Interfaces* **5**, 10294–10301 (2013).
14. W. J. Koros, C. Zhang, Materials for next-generation molecularly selective synthetic membranes. *Nat. Mater.* **16**, 289–297 (2017).
15. W. Kopec, D. A. Köpfer, O. N. Vickery, A. S. Bondarenko, T. L. C. Jansen, B. L. de Groot, U. Zachariae, Direct knock-on of desolvated ions governs strict ion selectivity in K^+ channels. *Nat. Chem.* **10**, 813–820 (2018).
16. S. J. Warnock, R. Sujanani, E. S. Zofchak, S. Zhao, T. J. Dilenschneider, Engineering Li/Na selectivity in 12-Crown-4–functionalized polymer membranes. *Proc. Natl. Acad. Sci. U.S.A.* **118**, e2022197118 (2021).
17. T. Sata, T. Yoshida, K. Matsusaki, Transport properties of phosphonic acid and sulfonic acid cation exchange membranes. *J. Membr. Sci.* **120**, 101–110 (1996).
18. R. K. Nagarale, G. S. Gohil, V. K. Shahi, R. Rangarajan, Preparation and electrochemical characterizations of cation-exchange membranes with different functional groups. *Colloid. Surf. A Physicochem. Eng. Asp.* **251**, 133–140 (2004).
19. Y. Ji, H. Luo, G. M. Geise, Effects of fixed charge group physicochemistry on anion exchange membrane permselectivity and ion transport. *Phys. Chem. Chem. Phys.* **22**, 7283–7293 (2020).
20. A. A. Uliana, N. T. Bui, J. Kamcev, M. K. Taylor, J. J. Urban, J. R. Long, Ion-capture electrodialysis using multifunctional adsorptive membranes. *Science* **372**, 296–299 (2021).
21. C. Sheng, S. Wijeratne, C. Cheng, G. L. Baker, M. L. Bruening, Facilitated ion transport through polyelectrolyte multilayer films containing metal-binding ligands. *J. Membr. Sci.* **459**, 169–176 (2014).
22. M. Yoshikawa, H. Ogata, K. Sanui, N. Ogata, Active and Selective Transports of Anions through Poly(*N*-propenoyl-9-acridinylamine-*co*-acrylonitrile) Membrane. *Polym. J.* **15**, 609–612 (1983).

23. S. J. Lounder, A. Asatekin, Interaction-based ion selectivity exhibited by self-assembled, cross-linked zwitterionic copolymer membranes. *Proc. Natl. Acad. Sci. U.S.A.* **118**, e2022198118 (2021).
24. T. Luo, S. Abdu, M. Wessling, Selectivity of ion exchange membranes: A review. *J. Membr. Sci.* **555**, 429–454 (2018).
25. S. Wijeratne, M. L. Bruening, G. L. Baker, Layer-by-layer assembly of thick, Cu^{2+}-chelating films. *Langmuir* **29**, 12720–12729 (2013).
26. J. Fan, C. Boi, S. M. Lemma, J. Lavoie, R. G. Carbonell, Iminodiacetic acid (IDA) cation-exchange nonwoven membranes for efficient capture of antibodies and antibody fragments. *Membranes* **11**, 530 (2021).
27. K. Naka, Y. Tachiyama, K. Hagihara, Y. Tanaka, M. Yoshimoto, A. Ohki, S. Maeda, Synthesis and chelating properties of poly[(*N*,*N*-dicarboxymethyl)allylamine] derived from poly(allylamine). *Polym. Bull.* **35**, 659–663 (1995).
28. A. E. Martell, R. M. Smith, *Critical Stability Constants* (Springer, 1990), vol. 6.
29. E. R. Nightingale Jr., Phenomenological theory of ion solvation. Effective radii of hydrated ions. *J. Phys. Chem.* **63**, 1381–1387 (1959).
30. D. W. Smith, Ionic hydration enthalpies. *J. Chem. Educ.* **54**, 540 (1977).
31. H. Irving, R. J. P. Williams, The stability of transition-metal complexes. *J. Chem. Soc.* **1953**, 3192–3210 (1953).
32. S. S. Shiratori, M. F. Rubner, pH-dependent thickness behavior of sequentially adsorbed layers of weak polyelectrolytes. *Macromolecules* **33**, 4213–4219 (2000).
33. P. Vanýsek, Ionic conductivity and diffusion at infinite dilution. *CRC Handb. Chem. Phys.* **96**, 77–79 (1996).
34. F. Helfferich, *Ion Exchange* (McGraw-Hill, 1962).
35. X. Zhou, Z. Wang, R. Epsztein, C. Zhan, W. Li, J. D. Fortner, T. A. Pham, J. Kim, M. Elimelech, Intrapore energy barriers govern ion transport and selectivity of desalination membranes. *Sci. Adv.* **6**, eabd9045 (2020).
36. C. L. Ritt, J. R. Werber, M. Wang, Z. Yang, Y. Zhao, H. J. Kulik, M. Elimelech, Ionization behavior of nanoporous polyamide membranes. *Proc. Natl. Acad. Sci. U.S.A.* **117**, 30191–30200 (2020).
37. P. Długołecki, K. Nymeijer, S. Metz, M. Wessling, Current status of ion exchange membranes for power generation from salinity gradients. *J. Membr. Sci.* **319**, 214–222 (2008).
38. G. M. Geise, D. R. Paul, B. D. Freeman, Fundamental water and salt transport properties of polymeric materials. *Prog. Polym. Sci.* **39**, 1–42 (2014).
39. J. G. Wijmans, R. W. Baker, The solution-diffusion model: A review. *J. Membr. Sci.* **107**, 1–21 (1995).
40. S. B. Sigurdardottir, R. M. DuChanois, R. Epsztein, M. Pinelo, M. Elimelech, Energy barriers to anion transport in polyelectrolyte multilayer nanofiltration membranes: Role of intra-pore diffusion. *J. Membr. Sci.* **603**, 117921 (2020).
41. H. B. Park, J. Kamcev, L. M. Robeson, M. Elimelech, B. D. Freeman, Maximizing the right stuff: The trade-off between membrane permeability and selectivity. *Science* **356**, 1137 (2017).
42. G. Z. Ramon, M. C. Y. Wong, E. M. V. Hoek, Transport through composite membrane, Part 1: Is there an optimal support membrane? *J. Membr. Sci.* **415-416**, 298–305 (2012).
43. B. J. Zwolinski, H. Eyring, C. E. Reese, Diffusion and membrane permeability. *J. Phys. Colloid Chem.* **53**, 1426–1453 (1949).
44. B. C. Welch, O. M. McIntee, T. J. Myers, A. R. Greenberg, V. M. Bright, S. M. George, Molecular layer deposition for the fabrication of desalination membranes with tunable metrics. *Desalination* **520**, 115334 (2021).
45. F. Li, L. Li, X. Liao, Y. Wang, Precise pore size tuning and surface modifications of polymeric membranes using the atomic layer deposition technique. *J. Membr. Sci.* **385–386**, 1–9 (2011).
46. M. Majumder, N. Chopra, B. J. Hinds, Effect of tip functionalization on transport through vertically oriented carbon nanotube membranes. *J. Am. Chem. Soc.* **127**, 9062–9070 (2005).
47. S. Bing, W. Xian, S. Chen, S. Ma, Bio-inspired construction of ion conductive pathway in covalent organic framework membranes for efficient lithium extraction. *Matter* **4**, 2027–2038 (2021).
48. S. U. Hong, R. Malaisamy, M. L. Bruening, Separation of fluoride from other monovalent anions using multilayer polyelectrolyte nanofiltration membranes. *Langmuir* **23**, 1716–1722 (2007).
49. Gaussian 16, Revision C.01, M. J. Frisch, G. W. Trucks, H. B. Schlegel, G. E. Scuseria, M. A. Robb, J. R. Cheeseman, G. Scalmani, V. Barone, G. A. Petersson, H. Nakatsuji, X. Li, M. Caricato, A. V. Marenich, J. Bloino, B. G. Janesko, R. Gomperts, B. Mennucci, H. P. Hratchian, J. V. Ortiz, A. F. Izmaylov, J. L. Sonnenberg, D. Williams-Young, F. Ding, F. Lipparini, F. Egidi, J. Goings, B. Peng, A. Petrone, T. Henderson, D. Ranasinghe, V. G. Zakrzewski, J. Gao, N. Rega, G. Zheng, W. Liang, M. Hada, M. Ehara, K. Toyota, R. Fukuda, J. Hasegawa, M. Ishida, T. Nakajima, Y. Honda, O. Kitao, H. Nakai, T. Vreven, K. Throssell, J. A. Montgomery Jr., J. E. Peralta, F. Ogliaro, M. J. Bearpark, J. J. Heyd, E. N. Brothers, K. N. Kudin, V. N. Staroverov, T. A. Keith, R. Kobayashi, J. Normand, K. Raghavachari, A. P. Rendell, J. C. Burant, S. S. Iyengar, J. Tomasi, M. Cossi, J. M. Millam, M. Klene, C. Adamo, R. Cammi, J. W. Ochterski, R. L. Martin, K. Morokuma, O. Farkas, J. B. Foresman, and D. J. Fox, Gaussian, Inc., Wallingford CT, 2016.
50. H. B. Schlegel, Optimization of equilibrium geometries and transition structures. *J. Comput. Chem.* **3**, 214–218 (1982).
51. V. Barone, M. Cossi, Quantum calculation of molecular energies and energy gradients in solution by a conductor solvent model. *J. Phys. Chem. A* **102**, 1995–2001 (1998).
52. J. Tomasi, B. Mennucci, R. Cammi, Quantum mechanical continuum solvation models. *Chem. Rev.* **105**, 2999–3094 (2005).
53. B. Honarparvar, S. Kanchi, K. Bisetty, Theoretical insights into the competitive metal bioaffinity of lactoferrin as a metal ion carrier: A DFT study. *New J. Chem.* **43**, 16374–16384 (2019).
54. R. A. Robinson, R. H. Stokes, *Electrolyte Solutions: Second Revised Edition* (Dover Publications Inc., 1959).
55. K. A. Dill, S. Bromberg, D. Stigter, *Molecular Driving Forces: Statistical Thermodynamics in Biology, Chemistry, Physics, and Nanoscience* (Garland Science, ed. 2, 2010).
56. W. S. Winston, K. K. Sirkar, *Membrane Handbook* (Springer Science+Business Media, 1992), vol. 1.

Acknowledgments: We thank X. Zhou and R. Epsztein for valuable discussions that led to this paper. Yale Institute of Nanoscale and Quantum Engineering (YINQE) provided profilometry equipment. We thank J. Karosas for assistance with ICP-MS at the Yale Analytical and Stable Isotope Center (YASIC). Yale Chemical and Biophysical Instrumentation Center (CBIC) provided NMR and FTIR equipment. We thank M. Li for assistance with SEM-EDS at Yale West Campus Materials Characterization Core. Yale Glass Shop provided diffusion cells. **Funding:** This work was supported by the U.S. National Science Foundation (NSF) and U.S.-Israel Binational Science Foundation (BSF) under award no. CBET-2110138 (transport experiments), the NSF Engineering Research Center for Nanotechnology-Enabled Water Treatment (NEWT) under award no. EEC-1449500 (synthesis and material characterization), and the Center for Enhanced Nanofluidic Transport (CENT), an Energy Frontier Research Center funded by the U.S. Department of Energy, Office of Science, Basic Energy Sciences under award no. DE-SC0019112 (simulations). We also acknowledge the Abel Wolman Fellowship from the American Water Works Association awarded to R.M.D. **Author contributions:** R.M.D., R.V., and M.E. conceptualized and designed the study. R.M.D., J.Y., C.J.P., and X.Z. conducted polymer synthesis. R.M.D., J.Y., and C.J.P. performed experiments, and M.H. performed simulations. All authors discussed results. R.M.D., J.Y., and C.J.P. performed data analysis and visualization. R.M.D., M.H., and M.E. wrote the manuscript, with all authors contributing to manuscript editing. **Competing interests:** The authors declare that they have no competing interests. **Data and materials availability:** All data needed to evaluate the conclusions in the paper are present in the paper and/or the Supplementary Materials.

Submitted 23 October 2021
Accepted 11 January 2022
Published 4 March 2022
10.1126/sciadv.abm9436

ScienceAdvances

Designing polymeric membranes with coordination chemistry for high-precision ion separations

Ryan M. DuChanoisMohammad HeiranianJason YangCassandra J. PorterQilin LiXuan ZhangRafael VerduzcoMenachem Elimelech

Sci. Adv., 8 (9), eabm9436. • DOI: 10.1126/sciadv.abm9436

Science Advances (ISSN) is published by the American Association for the Advancement of Science. 1200 New York Avenue NW, Washington, DC 20005. The title *Science Advances* is a registered trademark of AAAS.